International Journal of Pharmaceutics 642 (2023) 123108

Contents lists available at ScienceDirect

International Journal of Pharmaceutics

journal homepage: www.elsevier.com/locate/ijpharm

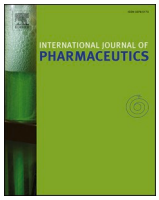

Development of dissolving microneedles for intradermal delivery of the long-acting antiretroviral drug bictegravir

Chunyang Zhang, Lalitkumar K. Vora, Ismaiel A. Tekko, Fabiana Volpe-Zanutto, Ke Peng, Alejandro J. Paredes, Helen O. McCarthy, Ryan F. Donnelly *

School of Pharmacy, Queen's University Belfast, Medical Biology Centre, 97 Lisburn, Road, Belfast BT9 7BL, UK

ARTICLE INFO

Keywords:
Human immunodeficiency virus
Bictegravir
Nanosuspensions
Microneedles

ABSTRACT

Oral administration and intramuscular (IM) injection are commonly recommended options for human immunodeficiency virus (HIV) treatment. However, poor patient compliance due to daily oral dosing, pain at injection sites and the demand for trained healthcare staff for injections limit the success of these administration routes, especially in low-resource settings. To overcome these limitations, for the first time, we propose novel bilayer dissolving microneedles (MNs) for the intradermal delivery of long-acting nanosuspensions of the antiretroviral (ARV) drug bictegravir (BIC) for potential HIV treatment and prevention. The BIC nanosuspensions were prepared using a wet media milling technique on a laboratory scale with a particle size of 358.99 ± 18.53 nm. The drug loading of nanosuspension-loaded MNs and BIC powder-loaded MNs were 1.87 mg/0.5 cm^2 and 2.16 mg/0.5 cm^2, respectively. Both dissolving MNs exhibited favorable mechanical and insertion ability in the human skin simulant Parafilm® M and excised neonatal porcine skin. Importantly, the pharmacokinetic profiles of Sprague Dawley rats demonstrated that dissolving MNs were able to intradermally deliver 31% of drug loading from nanosuspension-loaded MNs in the form of drug depots. After a single application, both coarse BIC and BIC nanosuspensions achieved sustained release, maintaining plasma concentrations above human therapeutic levels (162 ng/mL) in rats for 4 weeks. These minimally invasive and potentially self-administered MNs could improve patient compliance, providing a promising platform for the delivery of nanoformulated ARVs and resulting in prolonged drug release, particularly for patients in low-resource settings.

1. Introduction

Human immunodeficiency virus (HIV) remains a global public health issue. At the end of 2020, it was estimated that 37.7 million people were living with HIV, and 680,000 people died of AIDS-related illnesses (Global, 2022). Since the emergence of antiretroviral treatment (ART), the mortality and morbidity related to this epidemic have considerably decreased and the quality of life of HIV-infected patients has improved (Mayer and Venkatesh, 2010). However, sub-Saharan Africa remains the epicenter of the HIV global epidemic, accounting for >70% of the infectious load worldwide (Kharsany and Karim, 2016). Therefore, the success of the management of the spread of HIV in sub-Southern Africa may significantly decrease the global burden of HIV infections. One of the means to combat HIV infection is to develop long-acting ARV drugs, which require administration on a monthly, rather than daily, basis. The first long-acting injectable ARV regimen containing cabotegravir and rilpivirine (Cabenuva®) has shown a non inferior efficiency in maintaining HIV-1 suppression compared with conventional oral therapy (Swindells et al., 2020). However, the majority of people living with HIV are located in low- and middle-income countries, posing great challenges to implementing such innovative long-acting injectable formulations. Specifically, the delivery of long-acting formulations *via* IM injection requires trained healthcare workers, which may limit access to HIV treatment (Havlir and Gandhi, 2015). Due to the sensitivity of Cabenuva® to temperature, a cold chain at 2–8 °C is required during the shipment and storage of the drug (Thoueille et al., 2022). Thus, such injectable ARV formulations may not be available in countries with limited resources. The distance from health-care facilities and the lack of transportation are also concerning issues in developing countries (Palk et al., 2020). Furthermore, misuse and improper disposal of needles also present particular risks for the transmission of HIV and other blood-borne diseases (Vlahov et al., 2010). In addition, pain caused by

* Corresponding author at: Chair in Pharmaceutical Technology, School of Pharmacy, Queens University Belfast, Medical Biology Centre, 97 Lisburn Road, Belfast BT9 7BL, Northern Ireland, UK.
E-mail address: r.donnelly@qub.ac.uk (R.F. Donnelly).

https://doi.org/10.1016/j.ijpharm.2023.123108
Received 27 February 2023; Received in revised form 2 June 2023; Accepted 5 June 2023
Available online 8 June 2023

injection is commonly reported and is regarded as the main cause for the unacceptability of the products intended to use for 4- or 8-week treatment (Margolis et al., 2017). Consequently, the development of an improved drug delivery route for long-acting ARV drugs in developing countries, particularly in resource-limited settings, is an urgent issue.

Bictegravir (BIC) is a potent integrase strand transfer inhibitor (INSTI) developed by Gilead Science as a therapy for HIV-1-infected patients. This ARV drug was approved by the US Food and Drug Administration (FDA) in February 2018 as part of a fixed dose (50 mg) daily tablet (Biktarvy®) in combination with emtricitabine and tenofovir alafenamide. BIC is capable of binding to the integrase active site and blocking the strand transfer step of retroviral deoxyribonucleic acid (DNA) integration, which is essential in the HIV replication cycle. As the second generation of INSTI, BIC allows for fewer drug-drug interactions when it is administered with other agents (Lazerwith et al., 2022).

Dissolving microneedles (MNs) are promising devices intended to replace the conventional IM injection of ARV formulations, as they can be applied for minimally invasive intradermal delivery of micro- or nanoformulated drugs into the skin (Volpe-Zanutto et al., 2022). Compared with the parenteral administration route, such a self-administered drug delivery platform could overcome disadvantages, such as local pain, generation of sharp waste and the requirement for trained healthcare staff (Donnelly and Larrañeta, 2018; McAlister et al., 2021). However, fabrication of dissolving MNs loaded with crude micron-sized drug is challenging due to the difficulties of achieving a uniform drug distribution and high drug loading in aqueous polymeric blends used to form the dissolving MN matrix (Vora et al., 2018). To circumvent these limitations, nanosuspensions (interchangeably called nanocrystals) could be considered. Nanosuspensions are colloidal systems composed of submicron (<1 μm) pure drug particles, usually surrounded by a stabilizer layer (McGuckin et al., 2022; Abdelghany et al., 2019). A nanosuspension-loaded in the dissolving MNs may remain stable in the dry state of the polymeric MN matrix (Vora et al., 2018). Once MNs are inserted into the skin, the hydrophilic matrix of MNs dissolves quickly upon contact with interstitial fluid and the incorporated drug nanocrystals are then intradermally deposited as a depot and slowly released for absorption into the systemic circulation. If enough nanocrystals are deposited, the therapeutic plasma levels could potentially be maintained for prolonged periods (Tekko et al., 2020; Vora et al., 2022). Due to its hydrophobic nature, the drug is released slowly from the microdepots and then absorbed by the dermal microcirculation. Some particles with suitable particle sizes may also drain into thoracic lymphatic vessels because the particle size allows physical filtration into the lymphatic sinuses (Vora et al., 2022; Surve and Jindal, 2020). These dissolved drug could be slowly released into the systemic circulation from the lymphatic system, resulting in a long-acting ARV impact (Surve and Jindal, 2020; Vora et al., 2021). Currently, dissolving MNs have been investigated for the delivery of long-acting agents for the treatment of chronic diseases (Li et al., 2019; Rabiei et al., 2021). Recently, work indicating the potential of dissolving MNs used for intradermal delivery of ARV drugs for sustained release has also been published by our MN research team. Cabotegravir, rilpivirine and etravirine nanosuspensions were successfully delivered in this needle-free manner (Volpe-Zanutto et al., 2022; Mc Crudden et al., 2018; Rojekar et al., 2021; Tekko et al., 2022; Paredes et al., 2022; Moffatt et al., 2022). Consequently, these results have shown promise for the intradermal deposition of a hydrophobic ARV compound by such a delivery platform. In this work, for the first time, innovative bilayer dissolving MNs prepared with biocompatible polymers were developed for intradermal delivery of BIC nanosuspensions in a sustained manner for potential HIV prevention or, in combination with another long-acting drug, for HIV treatment.

2. Materials and methods

2.1. Materials

Poly(vinyl alcohol) (PVA) with a molecular weight of 9–10 kDa and poly(vinylpyrrolidone) (PVP) with molecular weights of 58 kDa and 360 kDa were purchased from Sigma Aldrich, Steinheim, Germany. Bidistilled glycerol was purchased from VWR International, Leicestershire, UK. BIC was purchased from Enke Pharma-tech Co., Ltd, Cangzhou, China. All other reagents used in this work were of analytical reagent grade.

2.2. Fabrication and rationalization of BIC nanosuspensions

BIC nanosuspensions were prepared *via* a wet media milling technique (Permana et al., 2020). Ceramic beads partially stabilized with yttria (type YTZP) with a diameter of 0.1–0.2 mm were used as milling media, which were obtained from Chemco (Guanfu, China). In brief, BIC powder, 4 magnetic stirring bars (12 × 6 mm) and 2 mL ceramic beads were transferred into a glass vial. Next, 7 mL of 1% w/w PVA (10 kDa) solution was added to the glass vial as a polymeric stabilizer. Subsequently, the glass vial was sealed and fixed in the center of a magnetic hotplate stirrer with double-sided adhesive tape. Then, the drug was milled at 1500 rpm overnight at room temperature. At predetermined time points, the nanosuspensions were separated from the beads using a stainless-steel sieve with 38 μm openings. For rationalization of the BIC nanosuspensions, the size of the milling media, milling time and the amount of BIC were taken into consideration. First, the particle size was rationalized based on the size of the beads, which were 0.1–0.2 mm and 0.4–0.6 mm. The effect of the milling time on particle size was also investigated. A 20 μl aliquot was taken from the glass vial at predetermined time points (2, 4, 8, 24 h) and the particle size and PDI of the nanosuspensions were immediately measured, as detailed in section 2.3.1. To determine the appropriate drug loading in the formulation, different amounts of drug were added to formulate BIC nanosuspensions. The details of the rationalization parameters are presented in Table 1. To concentrate the BIC nanosuspensions for the subsequent fabrication of nanosuspension-loaded dissolving MNs, deionized water in the aqueous nanosuspension formulation was removed by lyophilization with the addition of PVP (K 29–32) (70 mg) as a cryoprotectant. The details of lyophilization cycle are provided in the supplementary information (**Table S1.** The steps of the lyophilization cycle). The lyophilization cycle contained three main steps, including the freezing step, in which water was frozen. A primary drying step that removes ice crystals by sublimation. This process was performed at low temperature and pressure (Abdelwahed et al., 2006). Finally, the secondary drying step, involves the subsequent removal of any unfrozen water remaining within the sample by desorption, usually at evaluated temperatures and low pressure (Degobert and Aydin, 2021).

Table 1
Rationalization parameters of BIC nanosuspensions.

Mass of BIC (mg)	Milling time (Hours)	Bead diameter (mm)
200	2	0.1–0.2
200	4	0.1–0.2
200	8	0.1–0.2
200	24	0.1–0.2
200	24	0.4–0.6
150	24	0.1–0.2
250	24	0.1–0.2
300	24	0.1–0.2

2.3. Characterization of BIC nanosuspensions

2.3.1. Measurement of particle size, polydispersity index and zeta potential

Determinations of particle size and polydispersity index (PDI) were performed using dynamic light scattering (DLS) (NanoBrook Omni® analyzer, Brookhaven Instruments Corporation, New York, USA). The aqueous nanosuspensions were diluted 100 times with deionized water in a cuvette before the analysis process. The samples were then analyzed at a scattering angle of 90° for 180 s. Each measurement process was conducted at 25 °C in three replicates. Zeta potential was measured by electrophoretic mobility at the same time. For lyophilized nanosuspensions, a 5 mg aliquot of sample was reconstituted in 5 mL deionized water. The reconstituted nanosuspensions were characterized based on particle size, PDI and zeta potential.

2.3.2. Morphology of BIC nanosuspensions

To visualize the surface morphology of the nanosuspensions, an environmental scanning electron microscope (SEM) with a Quanta FEG 250 instrument (FEI, Hillsboro, OR, USA) was applied to obtain images of the sample at an acceleration voltage of 10–20 kV under vacuum conditions (8×10^{-5} mbar). Initially, a drop of resuspended nanosuspensions was added to the surface of the carbon-coated adhesive disk. Afterwards, the nanosuspensions were dried at room temperature prior to observation. The crude drug was also examined using SEM simultaneously.

2.3.3. Attenuated total reflectance Fourier transform infrared

In this study, attenuated total reflectance Fourier transform infrared spectroscopy (ATR-FTIR) (Accutrac FT/IR-4100™ Series, Jasco, Essex, UK) was performed to identify potential drug-excipient interactions in the raw formulation materials and nanosuspensions. Samples were clamped between the stage of the sample holder and a digital torque controller. The range of measurement was recorded from 4000 to 600 cm^{-1} and the resolution used in the analysis procedure was 4 cm^{-1}.

2.3.4. Differential scanning calorimetry analyses

Thermal analysis was used to assess the potential change in the physical state of BIC in lyophilized nanosuspensions. Different scanning calorimetry (DSC) studies of plain BIC, lyophilized nanosuspensions and physical mixtures were carried out on a Q100 differential scanning calorimeter (DSC 2920, TA Instruments, Surrey, UK). Briefly, samples (5–10 mg) were weighed and placed in standard aluminum pans and then sealed. An empty aluminum pan was utilized as a reference. The samples were exposed to temperature-controlled conditions in the range of 25–300 °C at a heating rate of 10 °C/min under nitrogen flow. The thermograms were recorded and analyzed to identify the physical state of the samples.

2.3.5. Powder X-ray diffraction

To determine the crystallographic structure, powder X-ray diffraction (XRD) patterns of the pure drug, lyophilized nanosuspensions and physical mixture were obtained and analyzed using a powder X-ray diffractometer (MiniFlex II, Rigaku Corporation, Kent, England). Copper K-β was used as X-ray energy in this equipment. Before measurement, the powdered sample was placed on a sheet of glass specimen holder with a depth of 1 mm. The sample was irradiated with a beam of X-rays and scanned within a 2θ range of 0-60° in continuous mode. The scanning speed was 2° per minute.

2.3.6. Drug content of BIC nanosuspensions

To investigate the drug content in the lyophilized nanosuspension formulation, an aliquot of 10 mg of lyophilized nanosuspensions was weighed and resuspended in 10 mL deionized water. Afterwards, the sample was sonicated in a water bath for 24 h to ensure that the nanosuspensions were completely resuspended. Then, the reconstituted nanosuspensions were diluted 20 times using acetonitrile, followed by centrifugation at 14800 rpm for 15 min. Meanwhile, polymers in the sample were precipitated with the addition of acetonitrile. The supernatant was taken and analyzed using the validated HPLC method described in section 2.5.9. The process was performed in triplicate, and the average drug content was calculated.

2.3.7. In vitro release

Separate *in vitro* release studies of pure BIC and nanosuspensions were conducted using a dialysis method (Permana et al., 2019). To achieve sink conditions, 1% w/v sodium lauryl sulfate (SLS) in PBS (pH 7.4) was selected as the release medium based on the solubility of BIC. The obtained release profiles of crude BIC and nanosuspensions were compared. In brief, the Spectrapro®, 12,000–14,000 molecular weight cutoff dialysis membrane (Spectrum Medical Industries, Los Angeles, CA, USA) was soaked in release medium for 1 h at 37 °C before use. Lyophilized nanosuspensions equivalent to 6.8 mg of the pure drug were suspended in 1 mL release media in a dialysis membrane. The sealed dialysis bags were each placed in 100 mL release medium at 37 °C in an orbital shaker (ISF-7199, Jeio Tech, Seoul, Korea) at 100 rpm. An aliquot of 1 mL medium was taken at predetermined time points and replaced with 1 mL fresh medium. The samples were filtered through 0.45 μm membrane filters and diluted with mobile phase before HPLC analysis.

2.4. Fabrication of bilayer BIC MNs

Dissolving MNs loaded with either BIC nanosuspensions or crude BIC powder were fabricated in a two-step process (Fig. 1). As mentioned in section 2.2, PVA (9–10 kDa) and PVP (58 kDa) were utilized as excipients during the preparation of BIC nanosuspensions, which will help form the matrix of the MN tips due to their nature as fairly glassy film-forming polymers with a long history of use in MN manufacture (Nguyen et al., 2018). Therefore, the amount of deionized water to be added to freeze-dried nanosuspensions was selected as the only variable to control the viscosity of the aqueous blends for MN tip preparation. As such, deionized water (270 mg) was transferred to lyophilized BIC nanosuspensions (350 mg) to obtain aqueous blends with a favorable viscosity for fabrication of the first layer of MNs. Concerning the manufacture of MN-incorporated crude BIC, a combination of aqueous polymer gels containing 12% w/w PVA (10 kDa) and 12% w/w PVP (58 kDa) was used. The resultant formulations were poured onto MN moulds (needle density of 16 × 16, 600 μm pyramidal needles with 250 μm column shaft, 300 μm width at base and 100 μm interspacing) (Cordeiro et al., 2020). Subsequently, the moulds loaded with MN tip formulations were subjected to a positive pressure of 5 bars for 2.5 min in a pressure chamber (Richmond Scientific, Chorley, UK) to fill the cavity of the moulds. Then, the excessive formulation on the moulds was carefully removed using the edge of a spatula, and filled moulds were placed back in a pressure chamber with the application of 5 bars until the formulation in the cavity was dry.

Baseplate casting was carried out approximately 8 h after the first layer was prepared. The formulation used for casting the second layer was composed of an aqueous gel of 30% w/w PVP (360 kDa) and 1.5% w/w glycerol. Initially, a preformed green ring was attached to the surface of the mould to hold the aqueous gel used for the subsequent baseplate casting (Paredes et al., 2022). Next, an aqueous baseplate gel (800 μl) was added to the green ring and centrifuged at 3500 rpm for 10 min. The filled moulds were allowed to dry for 48 h at room temperature. The prepared MNs were then peeled off from the moulds and the sidewalls were carefully removed using scissors. Finally, the MNs were placed in a 37 °C degree oven overnight before being stored in a sealed 24-well plate for further characterization.

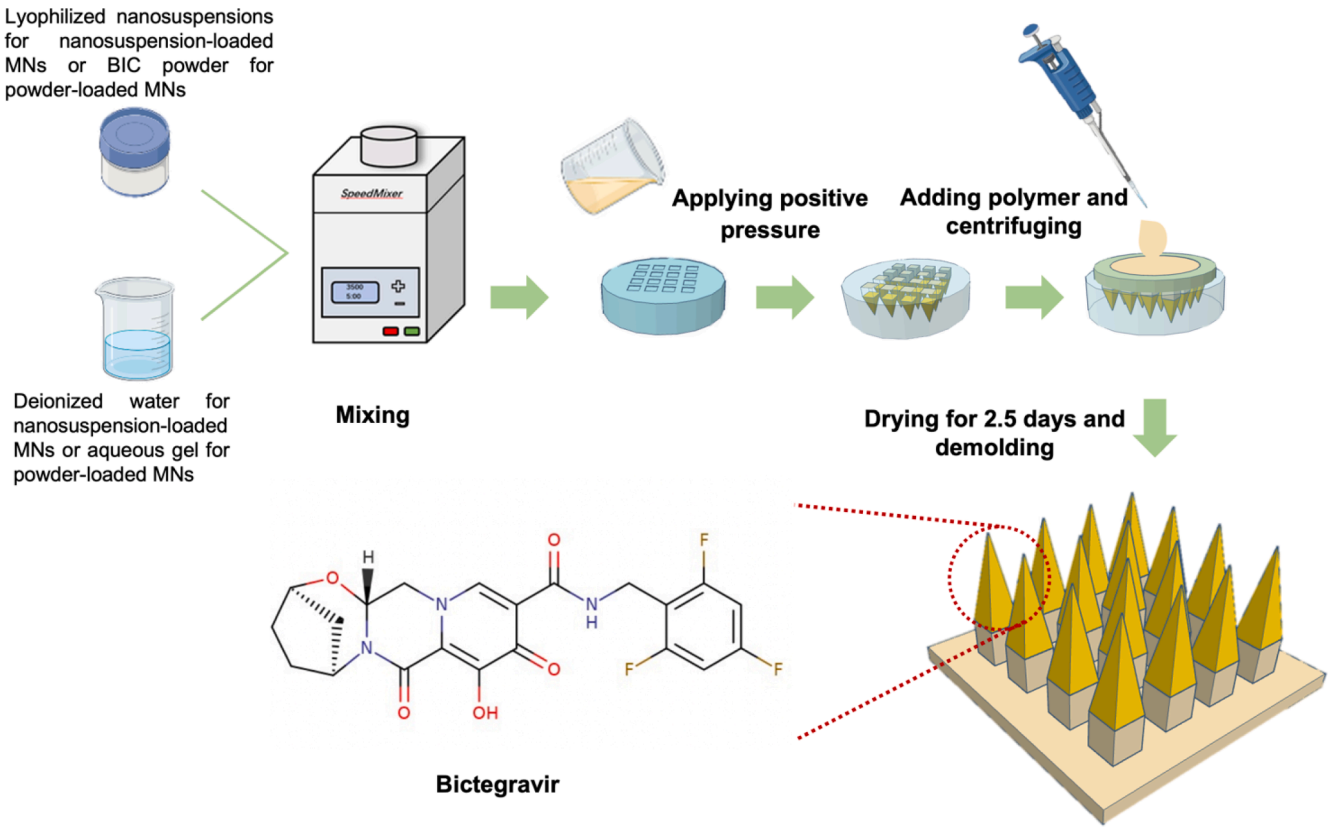

Fig. 1. Schematic presentation of the MN preparation process.

2.5. Characterization of dissolving MNs

2.5.1. Morphology of MNs

To visualize the morphology of the dissolving MNs, a Leica EZ4D digital microscope (Leica Microsystems, Milton Keynes, UK) and environmental SEM were applied to obtain images of the MNs. Prior to observation, the sample was attached to the carbon-coated adhesive disk and fixed onto an aluminum stub.

2.5.2. Evaluation of the effect of the MN preparation process on particle size

The tips of dried MNs containing BIC nanosuspensions were carefully cut off using scalpel and collected. Needle tips were then dissolved in deionized water and sonicated in a water bath for 24 h until a homogeneous suspension was obtained. Next, the particle size and PDI of the resuspended nanosuspensions were measured using DLS. The obtained data were compared with those of lyophilized nanosuspensions. The measurement was carried out in three replicates.

2.5.3. Evaluation of the mechanical properties of dissolving MNs

The experiment was carried out using a TA-TX2 Texture Analyzer (Stable Micro Systems, Surrey, UK) in compression mode, as described in a previous study (Garland et al., 2011; Donnelly et al., 2013). First, the initial heights of the dissolving MNs were measured and recorded with a Leica EZ4D digital stereo microscope (Leica Microsystems, Milton Keynes, United Kingdom). Afterwards, MNs were fixed onto the movable cylindrical Texture Analyzer probe using double-sided adhesive tape. The probe was programmatically moved with pre-test and post-test speeds of 1 mm/sec and a trigger force of 0.049 N. Subsequently, a force of 32 N was applied to the MNs against an aluminum block at a rate of 1 mm/sec for 30 s. Finally, the heights of the compressed MNs were visualized using a digital microscope again to determine the percentage height reduction. The percentage height reduction was calculated using **Equation 1**, where H_B refers to the height of the needles before compression and H_A refers to the height after compression.

$$\% \text{ Compression of the height} = (H_b\text{-}H_a)/H_b \times 100 \quad (1)$$

2.5.4. Insertion ability

To investigate MN insertion ability, Parafilm® M was utilized as a skin simulant as reported previously (Larrañeta et al., 2014). Specifically, Parafilm® M was folded into an eight-layer sheet approximately 1 mm thick, which was placed on aluminum foil-covered dental wax for support. The MNs were then inserted into the Parafilm® M layers using a TA-TX2 Texture Analyzer. Again, a force of 32 N was applied and held for 30 s at a speed of 1.19 mm/sec. The MNs were subsequently removed, and Parafilm® M was unfolded, followed by counting the number of holes in each layer under a Leica EZD4 digital microscope. The percentage of the holes created was calculated using **Equation 2**.

$$\% \text{ Holes in Parafilm® M} = \text{Number of holes observed/Number of microneedles} \times 100 \quad (2)$$

The skin insertion ability of dissolving MNs was evaluated using full-thickness neonatal porcine skin. Porcine skin was obtained from stillborn piglets and excised within 24 h of birth using a scalpel blade. The skin was then stored at −20 °C until use. Before insertion, the excised porcine skin was defrosted and equilibrated in PBS (pH = 7.4) for 30 mins at 37 °C. The shaved porcine skin was wiped with tissue to remove excessive buffer on the surface and placed on aluminum foil covered dental wax for support. Subsequently, dissolving MNs were inserted into the skin manually and held for 30 s. The insertion ability of the dissolving MNs was then observed using optical coherence tomography (OCT) (EX1301 VivoSight®, Michelson Diagnostics Ltd., Kent, UK).

2.5.5. Drug content determination in dissolving MNs

Drug content was determined from MNs containing BIC nanosuspension and unprocessed BIC powder. The whole MNs were individually dissolved in 5 mL deionized water and sonicated in a water bath for 24 h to ensure complete dissolution of the polymers. Afterwards, the reconstituted nanosuspensions were diluted 20 times using acetonitrile, followed by centrifugation at 14,800 rpm for 15 min. The supernatant was collected and analyzed for the drug content using the validated HPLC analytical method. The whole process was performed in five replicates.

2.5.6. Dissolution test

A dissolution study of the MNs was carried out using full-thickness excised neonatal porcine skin. The porcine skin was thawed, shaved, equilibrated in PBS for 30 min, and placed on PBS-soaked tissue paper (Tekko et al., 2022). Afterwards, the MN was manually inserted into the porcine skin and held for 30 s, followed by placing a 12 g cylindrical steel weight on the baseplate of the MNs to keep the MNs in the same position. The MNs were removed from the skin at determined time points and observed using a Leica EZ4D digital microscope.

2.5.7. Recovery test

To ensure the feasibility of the drug extraction method used in future *ex vivo* skin deposition studies, the recovery of BIC from full-thickness excised neonatal porcine skin was studied. First, the formulation of the nanosuspension-loaded MNs was prepared by reconstituting 104 mg of lyophilized BIC nanosuspensions in an aliquot of 80 mg deionized water and homogenized in a Speedmixer™ (Hauschild SpeedMixer®, Waterkamp, Germany) at 3500 rpm for 3 min. An aliquot of 10 mg of nanosuspension blend was added to a 2 mL Eppendorf® tube. Then, 1 cm^2 of full-thickness neonatal porcine skin was chopped into small pieces using a scalpel and mixed with a nanosuspension blend. The skin/nanosuspension mixture was vortexed and centrifuged to ensure that skin pieces were completely mixed by the nanosuspension blend. The Eppendorf® tube was subsequently placed in a 37 °C oven and incubated for 24 h. In contrast, for the control group, the Eppendorf® tubes containing solely a 10 mg mixture of bulk BIC and aqueous polymer (the same formulation as BIC nanosuspensions) were also incubated in a 37 °C oven for 24 h. All the samples were then subjected to the drug extraction process. Deionized water (500 μl) was initially added to Eppendorf® tubes to dissolve the residual polymer matrix in skin. Then, skin samples were disrupted in a Tissue Lyser (Qiagen, Ltd, Manchester, UK) for 10 min at 50 Hz. Afterwards, an aliquot of 1 mL acetonitrile was added to the resultant skin sample, followed by a second disruption using a Tissue Lyser for drug extraction. Finally, the skin samples were transferred to glass vials containing 3.5 mL acetonitrile and sonicated in a water bath for 30 mins. The samples were centrifuged prior to analysis with validated HPLC method (***Section 2.5.9***) after centrifugation. The recovery of BIC was calculated using **Equation (3)**. Five replications were performed for each group.

$$\%Recovery\ of\ BIC = \frac{Amount\ of\ BIC\ from\ experimental\ group\ (with\ skin)}{Amount\ of\ BIC\ from\ control\ group(without\ skin)} X100 \quad (3)$$

2.5.8. Ex vivo skin deposition studies

The study was carried out by using Franz diffusion cells (Fig. 7**A**). Full-thickness porcine skin was shaved and preequilibrated in PBS pH 7.4 for 30 mins prior to the experiment. SLS (1% w/v) in PBS was prepared as the release medium. After that, the skin surface was wiped with tissue paper and placed on aluminum foil-wrapped dental wax for support. The skin was subsequently attached to the donor compartment of the Franz cell using cyanoacrylate adhesive (Himawan et al., 2023). Dissolving BIC MNs were then inserted into the porcine skin with manual pressure and held for 30 s, followed by placing a 12 g cylindrical metal weight on the MN baseplate to ensure that the MNs remained *in situ*. The upper donor compartment and the sampling ports of the modified Franz cell were sealed with Parafilm® M. At determined time points (1 h, 6 h, 24 h), MNs were peeled off, and the skin was detached from the donor compartment. The skin was gently wiped with PBS-soaked tissue to remove residual formulation. Then, the area of skin where MNs were applied was collected in an individual 2 mL Eppendorf® tube. BIC was extracted and analyzed using the method mentioned in section 2.5.7. At determined sampling timepoints (1 h, 6 h, 24 h), release medium (300 μl) was withdrawn from the receptor compartment and filtered through a 0.2 μl membrane filter prior to HPLC analysis.

2.5.9. Pharmaceutical analysis of ex vivo samples

For *in vitro* and *ex vivo* studies, BIC was quantified using an Inertsil® (ODS3) C-18 column (250 mm × 4.6 mm, 5 μm) held at 40 °C and an Agilent 1200® series HPLC system (binary pump, degasser, autosampler) with UV detection at 260 nm. The mobile phase was composed of acetonitrile:deionized water containing 0.1% v/v trifluoracetic acid (60:40 v/v) with a flow rate of 0.8 mL/min, and the injection volume was 50 μl. The calibration curve was estimated using least squares linear regression analysis within a range of 0.625–50 μg/mL (R^2 = 0.9999). The analytical method was validated according to the International Council on Harmonization (ICH) Q2(R1) guidelines.

2.5.10. In vivo studies

Dissolving MNs containing BIC nanosuspensions and coarse BIC were separately applied to the backs of Sprague-Dawley rats to evaluate intradermal deposition and systemic delivery of BIC over a period of 4 weeks. Female Sprague-Dawley rats (n = 18) at 10–12 weeks of age (average body weight of 271.83 ± 24.59 g) were utilized throughout the *in vivo* study. This study was approved by the Committee of the Biological Services Unit (BSU), Queen's University Belfast. The work was conducted under Project License PPL 2903 and Personal License PIL 1892, PIL 1747 and PIL 2056 obtained from the UK Home Office. All experiments were conducted based on the policy of the Federation of European Laboratory Animal Science Associations and the European Convention for the protection of vertebrate animals used for experimental and other scientific purposes, implementing the principles of the 3Rs (replacement, reduction and refinement). Prior to commencement of experimentation, rats were acclimatized to conditions within the BSU for a minimum of 7 days.

As shown in Table 2, three cohorts of rats were used in this study (6 rats per cohort), including two MN cohorts and IM control cohort, investigating two different MN formulations, the first of which was applied with BIC nanosuspension-loaded MNs and the second MN cohort was applied with the MNs incorporated with crude BIC. In each cohort, four MN array patches were applied to each rat. For the IM control cohort, each rat received BIC nanosuspensions by IM injection.

To calculate the dose required to be administered for control and therapeutic purposes, the given dose (8 mg/kg) was obtained, which covered a period of 16 days based on a human oral dose of 50 mg/day (0.5 mg/kg/day), assuming a mean human weight of 70 kg and a rat weight of 250 g. The bioavailability of BIC is 70% after oral administration (Lu et al., 2021). The formulation for IM injection was prepared by dissolving 40 mg of BIC lyophilized nanosuspensions in 960 μl of sterilized water. A total of 100 μl of resuspended nanosuspensions was then administered to each rat.

Table 2
In vivo study plan showing the treatment cohort design for a single application.

Treatment cohorts		
Nanosuspension-loaded MNs	**Powder-loaded MNs**	**IM injection**
1 MN = 1.87 mg (4 MN = 7.48 mg)	1 MN = 2.16 mg (4 MN = 8.64 mg)	8.96 mg/kg (2.24 mg per rat)

2.5.11. Extraction of plasma and drug

Healthy female Sprague-Dawley rats were culled and blood was collected into heparinized tubes following cardiac puncture. This control blood was used for assay method development and optimization. To separate plasma from the blood, the tubes were centrifuged at 3000 relative centrifugal force (RCF) for 10 min at 4 °C. An aliquot of 90 µl rat plasma was then transferred to 1.5 mL Eppendorf® tubes. Aliquots of 10 µl BIC standard solution were added to blank plasma and vortexed for 15 min at 750 rpm. Afterwards, an aliquot of 300 µl acetonitrile was added into Eppendorf® tubes containing the plasma and BIC solution mixture, followed by vortexing for 15 min at 1500 rpm. The supernatant was taken for HPLC injection after centrifugation at 14800 rpm for 15 min by an Eppendorf MiniSpin® centrifuge (Eppendorf UK Ltd., Stevenage, United Kingdom).

2.5.12. Pharmaceutical analysis of in vivo samples

For *in vivo* studies, BIC was quantified from rat plasma using an Inertsil® (ODS3) C-18 column (250 mm × 4.6 mm, 5 µm) held at 40 °C and Agilent 1260® series HPLC system (quaternary pump, degasser, autosampler) partnered with an Agilent 1260® Infinity II mass spectrometry detector. Analytes were ionized using electrospray in positive ion mode (+), with BIC (Mw = 449.4) detected at a mass-to-charge ratio (*m/z*) of 450.4. The capillary voltage was established at 4 kV, drying gas temperature at 300 °C, drying gas flow at 11 L/min and the nebulizer pressure at 15 psi. Nitrogen was utilized as the source vapor and was maintained at 100 psi. The mobile phase was composed of acetonitrile: deionized water containing 0.1%v/v trifluoracetic acid (60:40 v/v) with a flow rate of 0.6 mL/min and the injection volume was 20 µl. BIC standard solutions were spiked in blank rat plasma, achieving a concentration range of 150–1250 ng/mL in blank plasma. The calibration curve was estimated using least squares linear regression analysis with a R^2 of 0.9965. The LoD and LoQ were 11.76 and 35.63 ng/mL, respectively. The analytical method was validated according to the US FDA bioanalytical guidelines.

2.5.13. Pharmacokinetic analysis

Basic pharmacokinetic parameters were calculated following a single MN application. Noncompartmental pharmacokinetic analysis of the plasma concentration profiles was applied using PK Solver. The maximum plasma concentration (C_{max}) of BIC was observed, and the time of maximum concentration (T_{max}) was determined by inspection of the raw data. The area under the curve (AUC), in this case, the plasma concentration–time curve from time zero ($t = 0$) to the last experimental time point (t = 28 d) ($AUCt_{0-\ final}$) for each rat cohort in each of the *in vivo* experimental designs, was calculated using the linear trapezoidal method. In the linear trapezoidal method, the AUC between two time intervals ($t_2 - t_1$) and their corresponding concentrations ($C_1 + C_2$) was calculated using **Equation 4.**

$$\text{AUC } t_{0\text{-final}} = 1/2\ (C_1+C_2)\ (t_2-t_1) \quad (4)$$

The relative bioavailability (F) of BIC after intradermal delivery of BIC-loaded dissolving MNs compared with IM injection was calculated using the following equation. The relative bioavailability was defined by comparing the AUC of BIC in plasma after the administration of two different formulations of the same compound (e.g., MNs vs. IM injection), where AUC_{MN} is the AUC of plasma from BIC nanosuspension-loaded MN administration and AUC_{IM} is the AUC of plasma from IM injection of BIC nanosuspensions. Furthermore, the total dose delivered from MNs and drug delivery efficiency were also calculated using following equations.

$$\%\ F = (AUC_{MN} \times dose_{IM})/(AUC_{IM} \times dose_{MN}) \times 100 \quad (5)$$

$$\text{Total dose delivered from MNs} = \%\ F \times \text{Dose MN} \quad (6)$$

$$\%\ \text{Delivery efficiency of MNs} = \text{Dose delivered/Dose of MNs} \times 100 \quad (7)$$

2.5.14. Estimation of human patch size

Using the mean plasma concentration–time data and F value obtained between MNs and IM injection, the patch size was estimated based on the pharmacokinetic study evaluating a single-dose administration of BIC nanosuspension loaded MNs and BIC nanosuspensions IM injection (Moffatt et al., 2022; Naser et al., 2023). The F ratio of BIC delivered from MNs with reference to IM injection was approximately 29%. This indicated that the amount of drug delivered by the four MNs was 2.19 mg (application area of 2 cm^2). Therefore, the amount of drug delivered per cm^2 was 1.09 mg. Additionally, the cautious estimation of MN patch size for humans was also predicted upon *ex vivo* skin deposition of BIC in neonatal porcine skin. Clinical trials have evaluated 10-day monotherapy with BIC oral tablets in HIV-1-infected adults. The dose of 5 mg BIC per day was non inferior to the normal oral dose level (50 mg per day), achieving a 95% inhibitory concentration (IC_{95}) (162 ng/mL) in the human body (Gallant et al., 1988). Therefore, 5 mg/day is adapted as an oral dose for BIC MN patch size estimation. The oral bioavailability of BIC has been estimated to be approximately 70% (Lu et al., 2021). The total amount of drug required for 30 days was 105 mg. To achieve the equivalent amount of drug delivered from the dissolving MN within 30 days, the size of human patches was estimated based on the amount of drug delivered per cm^2, considering that the area of each MN patch used in the study was 0.5 cm^2 (Tekko et al., 2022).

2.6. Statistical analysis

The data were analyzed using t tests and one-way ANOVA, followed by Tukey's multiple comparison post hoc test. $p < 0.05$ was considered a significant difference.

3. Results and discussion

3.1. Fabrication and rationalization of BIC nanosuspensions

In Fig. 2**A**, the particle size was significantly decreased to 358.99 ± 18.53 nm by using 2 mL milling beads (in a weight of 7.02 g) with a diameter of 0.1–0.2 mm in comparison to beads with a diameter of 0.4–0.6 mm ($p < 0.05$). Moreover, the particle size decreased significantly resulting from a longer milling time ($p < 0.05$). A narrow size distribution of the nanosized drug particles in the stabilizer was also achieved after a milling time of 24 h (Fig. 2**B**). A significant change in PDI from 0.28 ± 0.01 to 0.14 ± 0.02 was noted with such milling time ($p < 0.05$). Additionally, it was found that the drug content in the formulation had an impact on particle size and PDI. Fig. 2**C** illustrates that increased drug content causes significant growth in both particle size and PDI ($p < 0.05$). Compared to the drug loadings of 250 and 300 mg, both nanosuspension formulations containing 100 and 200 mg BIC exhibited fine particle sizes and relatively narrow particle size distributions. However, a drug loading of 200 mg was selected for the following characterizations and MN preparation since the maximal amount of drug was anticipated to be incorporated into dissolving MNs. The mechanism of drug nanosizing in the wet milling process can be described in two steps. Initially, crystals break rapidly because of more cracks and defects in larger crystals, which facilitate the spread of breakage (Malamatari et al., 2018). Following the initial stage of fast fracture, size reduction continues, but it remains at a slower rate until a plateau is reached (Plakkot et al., 2011). With prolonged milling time,

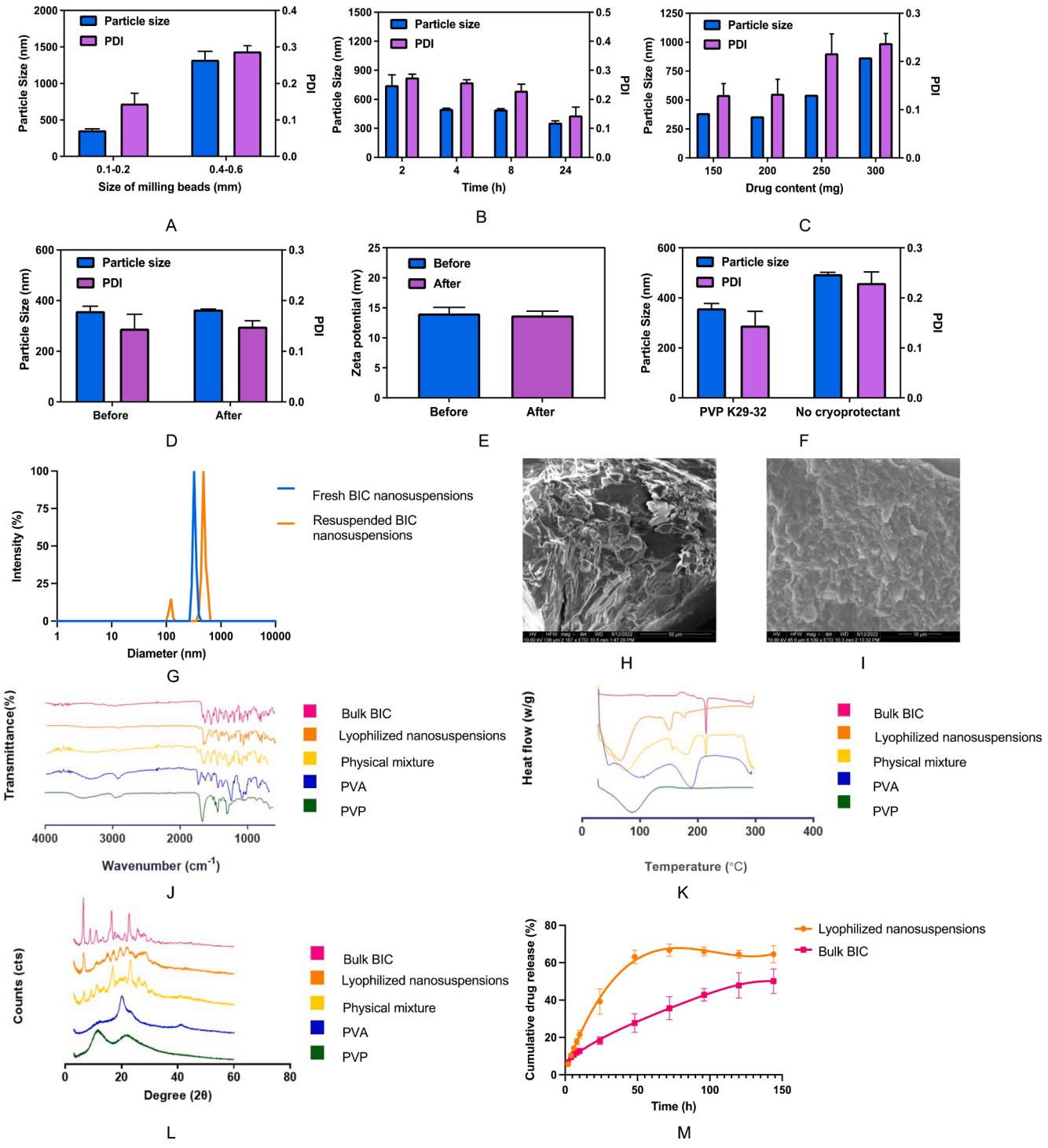

Fig. 2. Mean particle size and PDI of the nanosuspensions rationalized by applying milling beads with different sizes of milling media (A), milling time (B), and drug content (C); Mean particle size and PDI (D), and zeta potential (E) of the nanosuspensions before and after lyophilization; Mean particle size and PDI of the lyophilized nanosuspensions with and without cryoprotectant (F). (means + SDs., $n = 3$); Particle size distribution of BIC nanosuspensions before and after lyophilization (G). SEM images of the crude BIC powder (H) and the resuspended nanosuspension after lyophilization (I); scale bars are 50 μm and 10 μm respectively; ATR-FTIR spectra of the base materials, physical mixture of the base materials and lyophilized BIC nanosuspensions (J); DSC thermograms of the base materials, physical mixtures of the base materials and lyophilized BIC nanosuspensions (K); diffractograms of the base materials, physical mixtures of the base materials and lyophilized BIC nanosuspensions (L); *in vitro* drug release profile of BIC powder and lyophilized BIC nanosuspensions (M). (means ± SDs., $n = 3$).

the size of the drug particles decreases. The shear stress increases in the suspension (Plakkot et al., 2011). Therefore, attrition plays a dominant role in particle size reduction (Malamatari et al., 2018).

3.2. Characterization of BIC nanosuspensions

3.2.1. Particle size, polydispersion index and zeta potential

As shown in Fig. 2**D**, the particle size of the nanosuspensions remained almost the same before (358.99 ± 18.53 nm) and after lyophilization (387.52 ± 5.56 nm) ($p > 0.05$). The zeta potentials of the aqueous and freeze-dried nanosuspension formulations were + 14.07 ± 1.01 and + 13.77 ± 0.68 mV, respectively (Fig. 2**E**). Compared to the formulation containing cryoprotectant, a significant increase in particle size (495.03 ± 7.8 nm) was obtained for the formulation without cryoprotectant ($p < 0.05$) (Fig. 2**F**). Both fresh and reconstituted nanosuspensions exhibited relatively narrow size distributions (Fig. 2**G**). The added PVP served as a cryoprotectant to protect the system from potential aggregation. In addition, the same ratio of PVA and PVP used may contribute to the subsequent dissolving MN fabrication.

3.2.1.1. Morphology of BIC nanosuspensions. Fig. 2**H** and **I** present the morphologies of the crude drug and resuspended nanosuspensions, respectively. The bulk BIC powder was observed in micron-sized form, whereas the BIC nanoparticles were approximately nanosized, which was close to the particle size obtained from DLS.

3.2.1.2. Attenuated total reflectance Fourier transform infrared. As Fig. 2**J** displayed multiple peaks between 681 cm^{-1} and 827 cm^{-1} in the spectrum of bulk BIC due to aromatic C–H bending. Sharp peaks were also observed at approximately 1070 cm^{-1}, 1539 cm^{-1}, 1627 cm^{-1}, 1664 cm^{-1}, and 3234 cm^{-1}, corresponding to C-O stretching in the secondary amide, tertiary amide, C=O group and O–H group, respectively. All the characteristic peaks were present in both lyophilized BIC nanosuspensions and the physical mixture. Furthermore, no additional peaks were observed, indicating that there were no meaningful chemical interactions between the pure drug and excipients.

3.2.2. Differential scanning calorimetry analysis

As shown in Fig. 2**K**, the physical state of the pure drug, physical mixture, nanosuspensions and formulation excipients was determined. An intense endothermic peak appeared at 213 °C in the BIC powder and the physical mixture, corresponding to the melting point of drug crystals (Saxena et al., 2020). However, the endothermic peak was absent in the thermogram of the nanosuspension formulation. It was possible that there was adsorption of PVA onto the surface of the BIC nanoparticles, a type of physical interaction between the drug and excipients (Gulsun et al., 2018). The other possible reason for the absence of the melting peak is the transformation of the drug from a crystalline to an amorphous state. Apart from these characteristic peaks in the thermograms, no additional peaks were produced, therefore demonstrating that no chemical interactions were generated during the process of nanosuspension fabrication.

3.2.3. Powder X-ray diffraction

The diffractograms of the BIC powder, nanosuspension formulation and physical mixture are shown in Fig. 2**L**. Physical mixtures of PVA and PVP were used as controls. The X-ray diffraction pattern of crude BIC displayed characteristic sharp peaks at diffraction angles (2θ) of 6.4°, 16.4°, 22.6° and smaller peaks at 8.9°, 11°, 13.4°, 17.7°, 21.3° and 25.5°. PVA exhibited a characteristic peak at 20° and PVP was shown to be amorphous without any sharp peaks. The majority of distinctive peaks were retained in the physical mixture and lyophilized nanosuspensions, indicating that the crystalline state of BIC was partially preserved during the milling process. However, these peaks were dramatically diminished, probably resulting from the preparation approach of the nanosuspensions. This XRD result again reinforced the finding from the DSC study and showed that the resultant BIC nanosuspensions remained to some extent in the crystalline state rather than in a completely amorphous state. Similar results for other compounds were also found in the literature (Gulsun et al., 2018; Karakucuk and Celebi, 2020).

3.2.3.1. Drug content of BIC nanosuspensions. The drug content in the lyophilized BIC nanosuspensions was determined to ascertain the amount of drug contained in the freeze-dried product. The drug content of the lyophilized BIC nanosuspensions was 52.48 ± 1.32% w/w.

3.2.3.2. In vitro release study. The *in vitro* release profiles of plain BIC and lyophilized nanosuspensions are shown in Fig. 2**M**, reporting that the overall cumulative drug release of BIC was improved from the nanosuspension formulation compared to that from plain BIC within the duration of 144 h ($p > 0.05$). After 72 h, the nanosuspension formulation achieved the highest cumulative drug release of 66.77 ± 3.32% (4.54 ± 0.23 mg). Conversely, only 35.64 ± 6.11% cumulative drug release (2.42 ± 0.42 mg) was obtained at 72 h from the bulk BIC. Although there was no significant difference in total drug release, the nanosuspension formulation showed faster initial release. This profile indicated that the diffusion rate of the drug was enhanced due to the increased surface area to volume ratio after reduction of the particle size to nanoparticles (Khadka et al., 2014).

3.3. Fabrication of dissolving BIC MNs

During the MN manufacturing process, polymer selection is crucial for the formulation of dissolving MN arrays, which can be considered according to the following points. The polymeric excipients in dissolving MNs should possess favorable biocompatibility (Ahmed Saeed AL-Japairai et al., 2020). Considering the safety of the polymers used, the molecular weight should be relatively low (<60 kDa) so that they can be excreted from the body (Tekko et al., 2022). Furthermore, dissolving MNs are expected to be fabricated with high drug loading while maintaining sufficient mechanical properties. Finally, to reduce the time of MN application, MN tips and baseplates are expected to dissolve at different rates. Based on these points, low molecular weight PVA (9–10 kDa) and PVP (58 kDa) was chosen to prepare MN tips for faster dissolution while slow dissolving PVP (360 kDa) was used to prepare baseplates, achieving a programmed separation between drug-loaded MN tips and the supporting backing layer (Chang et al., 2020; Paredes et al., 2021).

Deionized water was added to lyophilized BIC nanosuspensions, forming an aqueous polymeric blend for subsequent MN tip preparation. However, the concentration of reconstituted BIC nanosuspensions is of significant importance. Concentrated BIC nanosuspensions led to a very viscous aqueous blend, which made it quite difficult to fill the cavity of the MN mould, while diluted nanosuspensions resulted in a nonhomogeneous distribution of the formulation on the surface of the mould due to the hydrophobicity of the silicone and subsequently reduced drug loading in the MN tips. Therefore, an incremental increase in the deionized water content in freeze-dried nanosuspensions was performed until homogeneous and sharp tips formed in the MN arrays. For baseplates of dissolving MNs, compared to the polymers used for dissolving MN tips, PVP with a high molecular weight in the baseplate formulation potentially exhibits a lower dissolution rate, thus achieving a programmed separation of drug-loaded tips with a blank baseplate (fast dissolving needle tips and slowly dissolving baseplate). Glycerol herein served as a plasticizer to provide flexibility of the supporting baseplate, avoiding fracture of the baseplate during the application process. Compared to traditional dissolving MNs containing APIs in whole needles, the localization of drugs in needle tips could effectively reduce drug waste since the needles cannot be fully inserted into the skin (Bok

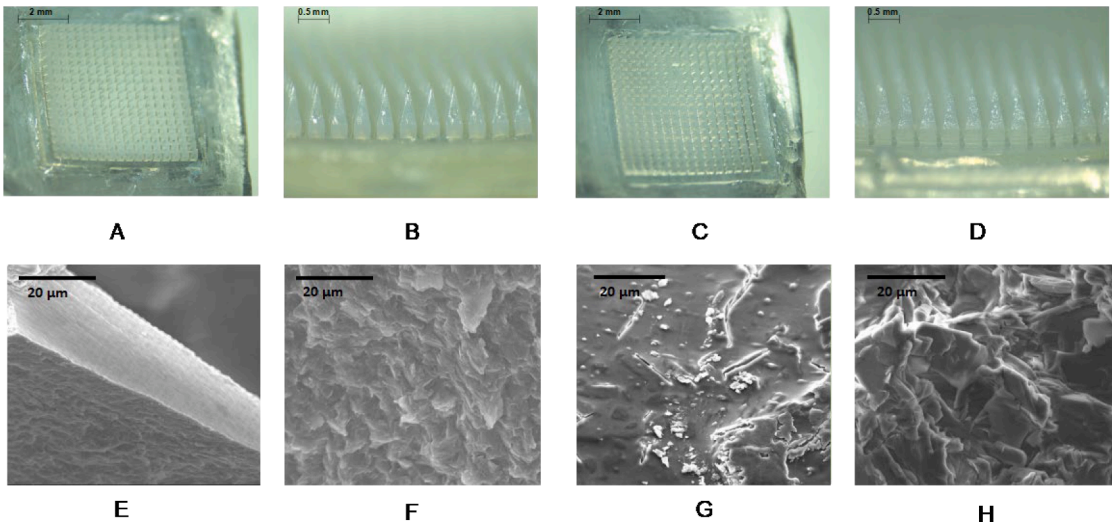

Fig. 3. Digital microscope images of the MNs containing BIC nanosuspensions (A and B) and crude BIC (C and D); scale bars are 2 mm (A and C) and 0.5 mm (B and D). The combination of PVA (9–10 kDa) and PVP (58 kDa) was chosen to prepare MN tips and PVP (360 kDa) was used to prepare baseplates, respectively. SEM images of the dissolving MNs containing BIC nanosuspensions (E and F) and crude BIC (G and H); scale bars are 20 μm.

et al., 2020; Dillon et al., 2019). Consequently, the MNs were fabricated *via* a two-step casting process to minimize drug loss during MN preparation and application, which improves drug delivery efficiency upon skin deposition (He et al., 2021).

3.4. Characterization of dissolving BIC MNs

3.4.1. Morphology of MNs

As displayed in Fig. 3 **A-D**, Both MNs were prepared with sharp tips and exhibited a homogeneous drug distribution in the first layer. SEM images (Fig. 3 **E-H**) revealed that BIC nanosuspension-loaded MNs exhibited a smooth MN surface without any obvious aggregation of nanoparticles. In contrast, a rough texture of MN tips loaded with micronized BIC particulates could be observed.

3.4.2. Evaluation of the mechanical properties of dissolving MNs

The representative percentage of the height reduction of MN tips following the compression test is indicated in Fig. 4**A and B**. The height of both dissolving MNs was reduced after compression by applying a force of 32 N. There was no significant difference in the height reduction between the nanosuspension-loaded MNs and drug powder-loaded MNs ($p > 0.05$). The percentages of height reduction were 7.89 ± 2.47% and 4.80 ± 4.27%, respectively. These results were similar to those of previously published work using PVA and PVP dissolving MNs with a height

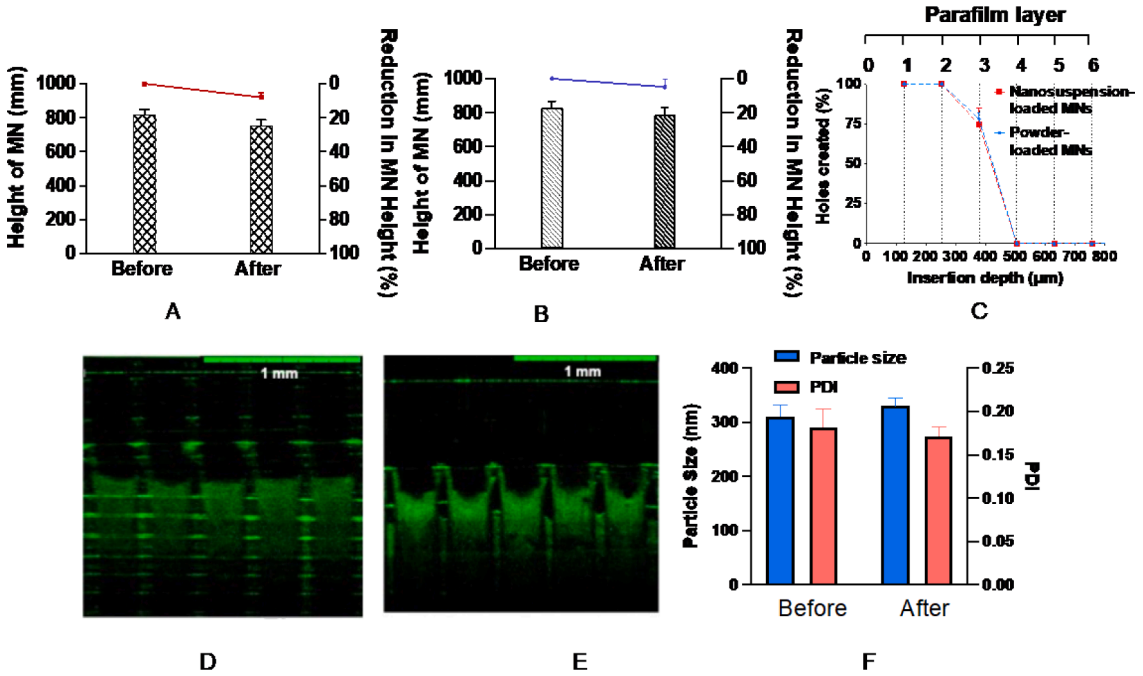

Fig. 4. Percentage of the height reduction of dissolving MNs containing nanosuspensions (A) and crude BIC (B) after the compression test; insertion depth and holes created by BIC dissolving MNs in the Parafilm® M insertion study (C) (means + SDs., $n = 3$); schematic representation of OCT equipment used for evaluation of insertion in Parafilm® M (D); OCT images of the BIC MNs inserted into porcine skin (E); mean particle size and PDI for BIC nanosuspensions, in a lyophilized form (before casting), and casting MNs using aqueous nanosuspensions, drying and dissolving MNs in deionized water (after casting) (F). (means + SDs., $n = 5$).

reduction of<10% (Nasiri et al., 2022). Therefore, both dissolving MNs were deemed likely to have sufficient mechanical robustness to be inserted into the skin.

3.4.3. Insertion ability

To evaluate the insertion ability of the dissolving MNs, the commercially available membrane Parafilm® M was utilized as a reproducible alternative to biological tissues, with the advantages of low cost, ease of access and safety of handling (Flaten et al., 2015). The percentage of the holes created in Parafilm® M is shown in Fig. 4**C**, which illustrates that both MNs possess the ability to penetrate the third layer of Parafilm® M. The mean thickness of each Parafilm® M is 126 ± 7 μm (Mc Crudden et al., 2018). Therefore, the total insertion depth of each MN patch was approximately 378 μm, which was equivalent to 63.0% of the BIC-loaded MN tip height. Both dissolving MNs reached all tip (256 tips) penetration of the first and second layers of Parafilm® M. In the 3rd layer, 74.34 ± 10.6% and 78.13 ± 3.51% of tips penetrated for nanosuspension-loaded MNs and powder-loaded MNs, respectively. Furthermore, excised neonatal porcine skin is one of the most commonly used *ex vivo* models for skin insertion studies due to its similar structure to human skin (Summerfield et al., 2015). OCT was also applied to visualize the insertion depth in full-thickness neonatal porcine skin and Parafilm® M. Fig. 4**D and E** revealed that most of the drug loaded MNs were inserted into Parafilm®M and neonatal porcine skin.

3.4.4. Evaluation of the effect of the MN preparation process on particle size

During the MN preparation process, the aggregation of nanoparticles may occur since high-speed homogenization and positive pressure were involved in the casting procedure (Bhakay et al., 2018). Hence, the nanoparticle-loaded tips were cut and dissolved in deionized water to characterize the nanoparticle properties. As shown in Fig. 4**F**, BIC nanoparticles exhibited an insignificant increase in particle size from 311 ± 20.21 to 330 ± 14.92 nm ($p > 0.05$) and an insignificant alteration in PDI from 0.182 ± 0.02 to 0.171 ± 0.01 ($p > 0.05$). These results revealed that the effect of the MN casting procedure on nanosuspension characterizations was minor, making them suitable for dissolving BIC MN preparation. Moreover, BIC nanosuspensions maintained intrinsic steric stabilization, allowing dissolving MNs to deliver nanosuspensions without significantly altering their original integrity.

3.4.5. Drug content determination in dissolving MNs

The drug contents in the two types of MNs were 1.87 ± 0.25 mg and 2.16 ± 0.34 mg for BIC nanosuspension MNs and BIC powder MNs, respectively.

3.4.6. Ex vivo skin dissolution test

Dissolving MNs are expected to display fast-dissolving behavior (in < 1 h ideally), which would greatly reduce the wearing time and thus be patient-friendly in a future clinical setting (Donnelly and Larrañeta, 2018; Mao et al., 2020). Dissolution of the dissolving MNs in full-thickness neonatal porcine skin was studied to predict the time required for the MNs to be dissolved in the skin. As illustrated in Fig. 5, the MN tips started to dissolve within 5 min. The dissolution continued for 10 min and 15 min. Until 20 min, the drug-loaded needle tips reached complete dissolution, even though they had a high hydrophobic drug content.

3.4.7. Recovery test

Drug content recovery studies were carried out to investigate the degree of the interactions between the drug and excised neonatal porcine skin, as well as the feasibility of the drug extraction method used further from full-thickness neonatal porcine skin. These results displayed a favorable recovery for BIC, demonstrating 102.10 ± 4.59% recovery. The results indicated that there were no interactions between BIC and excised porcine skin, and the extraction procedure was proven to be efficient.

3.4.8. Ex vivo skin deposition studies

Ex vivo skin deposition behavior of the dissolving MNs was performed to quantify the amount of BIC deposited in human skin simulant, full-thickness excised neonatal porcine skin (Fig. 6**A**). Upon skin insertion, the nanosuspensions incorporated in dissolving MNs were deposited as a depot and slowly released drug for absorption into the systemic circulation as they dissolved in the interstitial fluid (Donnelly and Larrañeta, 2018). As shown in Fig. 6 **E-H**, White depots were clearly observed in porcine skin after initial cleaning, showing the potential of dissolving MNs for intradermal delivery of BIC. For nanosuspension-loaded MNs, the total amount of BIC deposited in the skin reached 347.59 ± 51 μg/patch after 6 h of application, which is the highest amount of BIC deposited within 24 h. However, it was found that the amount of the drug deposited in the full-thickness porcine skin was 267.02 ± 46 μg/patch after 24 h. This can be attributed to some permeation of the BIC across the full-thickness skin. In contrast, although the amount of the drug deposited in porcine skin showed an increasing trend within 6 h, the amount of BIC deposited in full-thickness porcine skin from powder-loaded MNs was much lower than that from nanosuspension-loaded MNs. After 24 h, a total of 202.45 ± 39 μg of BIC was quantified in full-thickness porcine skin (Fig. 6**B**). As demonstrated in Fig. 6**C**, the amount of permeated drug from both dissolving BIC MNs increased as a function of time. After 24 h, 131.87 ±

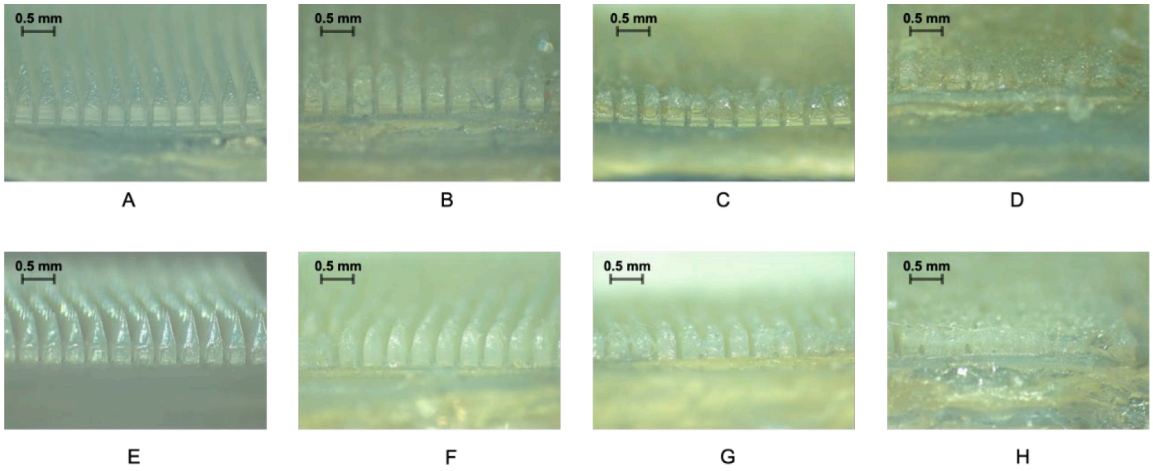

Fig. 5. Schematic presentation of the dissolution study in full-thickness porcine skin. Digital images of the dissolution of MNs containing nanosuspensions and crude powder at determined time points: showing time = 0 (A and E), 5 min (B and F), 10 min (C and G) and 20 min (D and H); scale bars are 0.5 mm.

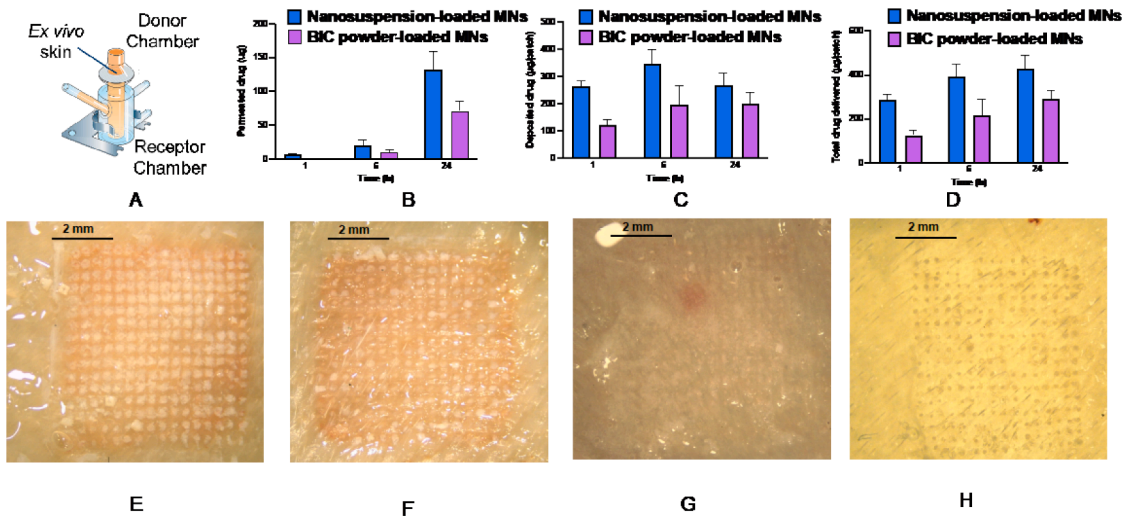

Fig. 6. Schematic representation of the Franz cell setup used for the *ex vivo* skin deposition study (A); Total amount of BIC delivered from the dissolving BIC MNs (B); Cumulative amount of BIC permeated across the full-thickness porcine skin after different durations (1 h, 6 h and 24 h) (C); Cumulative amount of BIC deposited in full-thickness porcine skin following application of dissolving MNs after different periods (1 h, 6 h and 24 h) (means + SDs, $n = 3$) (D); Digital images displaying the porcine skin following removal of dissolving MNs incorporated with nanosuspensions after 24 h (E) and the porcine skin appearance after cleaning with PBS-soaked tissue paper (F); the porcine skin following removal of dissolving MNs incorporated with drug powder after 24 h (G) and the porcine skin appearance after cleaning with PBS-soaked tissue (H).

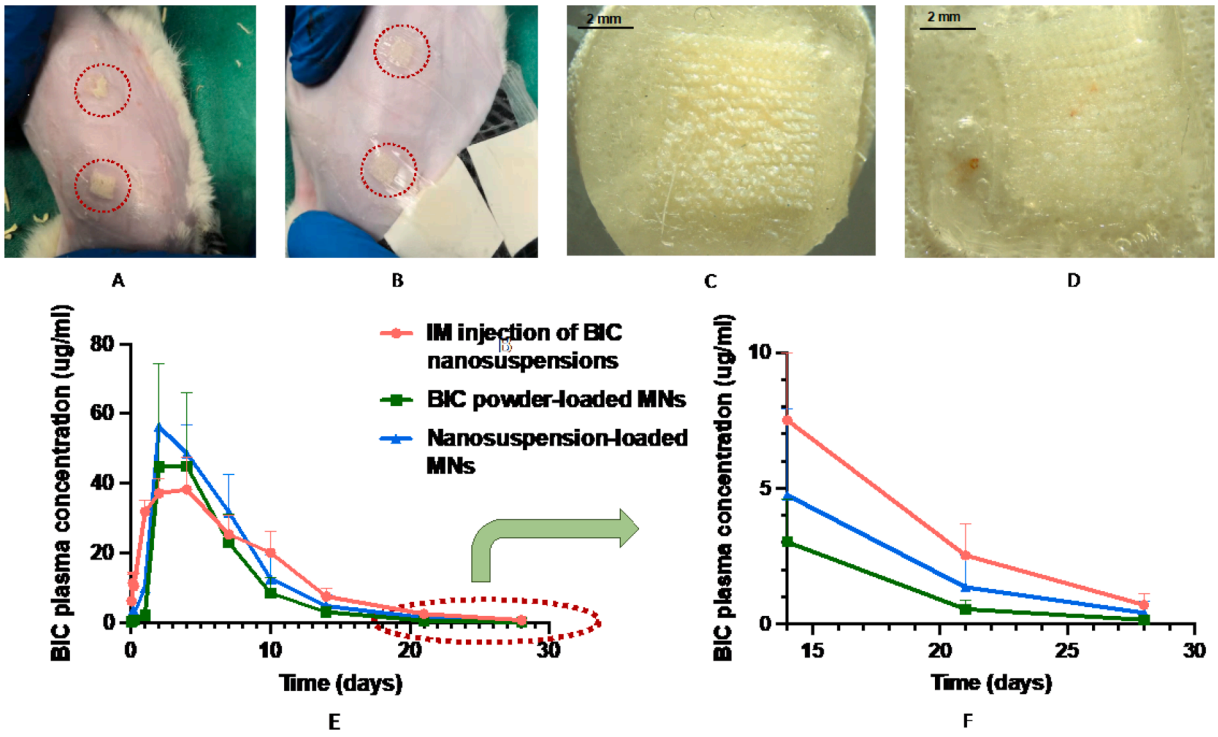

Fig. 7. Digital images following *in vivo* delivery of BIC nanosuspension-loaded MNs and BIC powder-loaded MNs (A) and (B); Digital images of MNs containing BIC nanosuspensions and BIC powder after application for 24 h (C) and (D). Comparative *in vivo* plasma pharmacokinetic profiles of BIC in Sprague-Dawley rats following a single dose application (E) (means + SDs, $n = 6$).

27.58 μg BIC permeated into the receiver compartment from MNs loaded with nanosuspensions, which was nearly twice the drug concentration obtained from crude powder containing dissolving MNs. The total amount of drug released from both dissolving MNs was determined by quantifying the drug in the receiver compartment and porcine skin. After 24 h of application, nanosuspension-loaded MNs led to superior *ex vivo* skin deposition compared to powder-loaded MNs, which were 427.98 ± 60.30 μg/patch and 292.77 ± 38.58 μg/patch, respectively ($p < 0.05$) (Fig. 6**D**).

3.4.9. *In vivo study*

As illustrated in Fig. 7**A and B**, the MN tip implants containing BIC nanosuspensions and BIC powder could be visualized from both MN cohorts at the site of MN application. The roots of MN array needles remained on the baseplates (Fig. 7**C and D**). The pharmacokinetic profiles of BIC from each cohort are presented in Fig. 7**E and F**. The therapeutic concentration of BIC in plasma was detectable after 1 h from the nanosuspension MN cohort and crude drug MN cohort (1.25 μg/mL and 0.23 μg/mL, respectively).

Table 3
Pharmacokinetic parameters of BIC from the MN cohort and IM control cohort (means ± SDs., $n = 6$).

Pharmacokinetic parameters	MN cohorts		Control cohort
	Nanosuspension-loaded MNs	Powder-loaded MNs	IM
C_{max} (μg/mL)	56.32 ± 17.88	44.89 ± 17.78	38.21 ± 9.16
T_{max} (days)	2	4	4
$AUC_{t0\text{-}28\ days}$ (μg.day/mL)	393.11 ± 77.90	301.14 ± 107.19	393.78 ± 131.21

The pharmacokinetic parameters of BIC in rats are presented in Table 3. Compared with the C_{max} from the IM control cohort at 4 days (38.21 μg/mL), the C_{max} of the nanosuspension-loaded MN cohort and BIC powder-loaded MN cohort were 56.32 μg/mL (at 2 days) and 44.89 μg/mL (at 4 days), respectively. Statistical analysis using Tukey's multiple comparison test showed no significant difference between all individual C_{max} values of the MN cohorts and the IM control cohort ($p > 0.05$). The plasma concentration was maintained above IC_{95} until 28 days for the nanosuspension MN cohort (0.42 μg/mL) and IM control cohort (0.71 μg/mL). The plasma concentration of the crude BIC MN cohort was slightly lower than the IC_{95} (162 ng/mL) at 28 days, which was 0.16 μg/mL. The shorter T_{max} obtained from nanosuspension-loaded MNs revealed that the BIC absorption rate from the MN application site was higher than that from IM injected depots (Tekko et al., 2022). This may be attributed to the difference in surface area between the nanosuspensions delivered *via* IM injection and dissolving MNs in rats. The nanosuspensions administered by IM injection were in a bolus form in the dense muscular tissue. However, each dissolving MN patch can potentially deliver 256 microdepots containing BIC nanosuspensions, which dramatically increases the surface area of the hydrophobic BIC compared with the 'large' depot delivered by IM injection. Higher absorption rates achieved by MN array patches have a potential advantage, not only in combating slower absorption rates resulting from inherited physiology and anatomy of the skin but also in the fact that they could help achieve therapeutic drug levels in plasma more quickly, which would provide immediate protection against HIV-1 infections (Tekko et al., 2022).

According to the $AUC_{t0\text{-}28}$ day, both MN cohorts exhibited a comparable pharmacokinetic profile compared with the IM cohort. The highest $AUC_{t0\text{-}28}$ days obtained from the IM control cohort was 393.78 ± 131.21 μg.day/mL. Similarly, the $AUC_{t0\text{-}28}$ days obtained from the nanosuspension-loaded MN cohort was 393.11 ± 77.90 μg.day/mL. The lowest $AUC_{t0\text{-}28}$ days obtained from the powder-loaded cohort was 301.14 ± 107.19 μg.day/mL. Statistical analysis using Tukey's multiple comparison test showed no significant difference between all individual $AUC_{t0\text{-}28}$ days of the MN cohorts and the IM control cohort ($p > 0.05$).

The relative bioavailabilities of BIC from nanosuspension-loaded MNs and BIC powder-loaded MNs were calculated based on IM injection and were 29.23 ± 9.76% and 19.38 ± 7.56%, respectively. As such, the dose delivered by dissolving MNs was cautiously estimated at 0.42 mg and 0.55 mg per MN array patch for those two MN groups, respectively. The drug delivery efficiency from the *in vivo* study was found to be 29.23 ± 9.76% and 19.38 ± 7.56% for MNs incorporated with BIC nanosuspensions and powder BIC, respectively. The higher relative bioavailability and delivery efficiency could be attributed to the increased surface area of the BIC nanosuspensions compared with crude drug particles, which enhances the dissolution rate and subsequent bioavailability. Therefore, the preliminary results from this small-scale proof-of-concept study show promise in combining dissolving MN array systems to achieve intradermal delivery of long-acting ARV nanosuspensions, which may potentially achieve and maintain HIV viral suppression for a prolonged period of time. Consequently, the requirement of daily dosing of oral ARV drugs may be avoided.

Although novel MN array patches have exhibited promising properties and capabilities in the intradermal delivery of long-acting BIC nanosuspensions, they still have some limitations to be addressed. The first is to improve MN array design to maximize drug loading and support successful insertion through optimization of MN tip dimensions and array density, thus resulting in a reduction in patch size for translation to human application. The second is the *in vivo* experimental environment (Tekko et al., 2022). According to the dissolution study presented in section 3.4.6, MNs could achieve complete dissolution within 20 mins. However, the MNs must be removed after 24 h of application from rats since the removal of the MNs requires anesthesia, which is permitted once within 24 h (Tekko et al., 2022). Therefore, this influences the evaluation of the real wearing time, which cannot provide an accurate estimation of the wearing time for patients. Furthermore, the biodistribution of BIC could be evaluated, especially in lymphatic tissues, in which HIV reservoirs reside (Wong and Yukl, 2016). By excising lymphatic organs, such as lymph nodes, spleen, and liver, the drug content in these organs can be quantified using HPLC-MS (Ramöller et al., 2022).

3.4.10. Estimation of the human patch size of MNs

According to an *in vivo* study, the required human patch size to deliver 105 mg of BIC was 96 cm^2. According to *ex vivo* skin deposition, to achieve a similar duration of exposure was achieved after single-dose administration. A patch size of 122.09 cm^2 would be required to provide a therapeutically relevant plasma concentration of BIC over a period of 30 days after a 24 h single application. However, both patch sizes would be inappropriate for human application, and a patch size of 22.4 cm^2 (from *in vivo* calculation) and 28.49 cm^2 (from *ex vivo* calculation) would be cautiously estimated to achieve a relevant plasma concentration over 7 days. These patch sizes are regarded within the acceptable range of the commercially available transdermal patch size, such as GlaxoSmithKline's Nicotinell® nicotine patches of 30 cm^2 and Janssen's Duragesic® CII (fentanyl) patches of 32 cm^2 and 42 cm^2 (Han and Das, 2015). Concerning the possibility of the self-administration of MN array patches, our research team has already performed a feasibility study to evaluate the self-administration of larger MN array patches with an area of 16 cm^2. The results showed that such an MN patch could be successfully administered by volunteers with a mean insertion depth across the entire large array comparable to that of the smaller patches (Ripolin et al., 2017).

The presented work has held promise to bridge the gap between ARV adherence and effectiveness, providing alternative options for patients who suffer from poor adherence to the daily pill regimen. This is the first study to intradermally deliver long-acting BIC nanosuspensions using an MN platform. However, some issues must be addressed prior to clinical translation. First, to accelerate the commercialization of MN-based products, a variety of GMP and QC tests need to be well established and validated by manufacturers. Furthermore, the safety of the materials used and the mechanism of metabolism are important. For dissolving MNs, the pathways of metabolism and elimination of the polymers in the human body need to be investigated, especially for long-term deposition in skin (Saxena et al., 2020). Future works include scalability studies of the formulation to investigate whether this formulation strategy is practical in larger manufacturing setups. User acceptability studies are also necessary prior to translating research to clinical studies.

4. Conclusion

In this work, BIC nanosuspensions were successfully prepared using a top-down method. Bilayer dissolving MNs containing nanosuspensions and crude drug were manufactured with satisfying mechanical properties and insertion ability. According to the *ex vivo* skin deposition study, >20% of the theoretical BIC located in MN tips was intradermally delivered into the excised neonatal porcine skin. The *in vivo* study illustrated that nanosuspension-loaded MNs showed a higher relative bioavailability than crude BIC-loaded MNs. This innovative drug delivery system has achieved comparable pharmacokinetic results compared with IM administration. The relevant therapeutic plasma concentration was obtained after a single MN application in Sprague-Dawley rats within a period of 28 days. Furthermore, a human MN patch size of 22.4 cm^2 (from *in vivo* calculation) and 28.49 cm^2 (from *ex vivo* calculation) were cautiously estimated to be able to maintain the plasma concentration above IC_{95} for 7 days in the human body. As such, BIC nanosuspension-loaded MNs are promising as a patient-friendly administration route for potential HIV pre-exposure prophylaxis or HIV treatment as a regimen of ARV drugs.

CRediT authorship contribution statement

Chunyang Zhang: Methodology, Investigation, Formal analysis, Writing – original draft, Writing – review & editing. **Lalitkumar K. Vora:** Methodology, Investigation, Supervision, Writing – review & editing. **Ismaiel A. Tekko:** Methodology, Investigation. **Fabiana Volpe-Zanutto:** Methodology, Investigation, Writing – review & editing. **Ke Peng:** Investigation. **Alejandro J. Paredes:** Methodology, Writing – review & editing. **Helen O. McCarthy:** Methodology, Resources. **Ryan F. Donnelly:** Conceptualization, Methodology, Supervision, Writing – review & editing, Resources, Project administration, Funding acquisition.

Declaration of Competing Interest

The authors declare that they have no known competing financial interests or personal relationships that could have appeared to influence the work reported in this paper.

Data availability

Data will be made available on request.

Acknowledgments

This work was supported by EPSRC grant EP/S028919/1 and Wellcome Trust grant WT094085MA.

Appendix A. Supplementary material

Supplementary data to this article can be found online at https://doi.org/10.1016/j.ijpharm.2023.123108.

References

Abdelghany, S., Tekko, I.A., Vora, L., Larrañeta, E., Permana, A.D., Donnelly, R.F., 2019. Nanosuspension-based dissolving microneedle arrays for intradermal delivery of curcumin. Pharmaceutics. 11, 1–13.

Abdelwahed, W., Degobert, G., Stainmesse, S., Fessi, H., 2006. Freeze-drying of nanoparticles: formulation, process and storage considerations. Adv. Drug Deliv. Rev. 58, 1688–1713.

Bhakay, A., Rahman, M., Dave, R.N., Bilgili, E., 2018. Bioavailability enhancement of poorly water-soluble drugs via nanocomposites: formulation–processing aspects and challenges. Pharmaceutics. 10, 86–148.

Bok, M., Zhao, Z.J., Hwang, S.H., Kang, H.J., Jeon, S., Ko, J., Jeong, J., Song, Y.S., Lim, E., Jeong, J.H., 2020. Effective dispensing methods for loading drugs only to the tip of DNA microneedles. Pharmaceutics. 12, 1–13.

Chang, H., Zheng, M., Chew, S.W.T., Xu, C., 2020. Advances in the formulations of microneedles for manifold biomedical applications. Adv Mater Technol. 5, 1–19.

Cordeiro, A.S., Tekko, I.A., Jomaa, M.H., Vora, L., McAlister, E., Volpe-Zanutto, F., Nethery, M., Baine, P.T., Mitchell, N., McNeill, D.W., Donnelly, R.F., 2020. Two-photon polymerisation 3D printing of microneedle array templates with versatile designs: application in the development of polymeric drug delivery systems. Pharm. Res. 37, 1–15.

Degobert, G., Aydin, D., 2021. Lyophilization of nanocapsules: instability sources, formulation and process parameters. Pharmaceutics. 13, 1112–1138.

Dillon, C., Hughes, H., O'Reilly, N.J., Allender, C.J., Barrow, D.A., McLoughlin, P., 2019. Dissolving microneedle based transdermal delivery of therapeutic peptide analogues. Int. J. Pharm. 565, 9–19.

Donnelly, R.F., Larrañeta, E., 2018. Microarray patches: potentially useful delivery systems for long-acting nanosuspensions. Drug Discov. Today 23, 1026–1033.

Donnelly, R.F., Singh, T.R.R., Alkilani, A.Z., McCrudden, M.T.C., O'Neill, S., O'Mahony, C., Armstrong, K., McLoone, N., Kole, P., Woolfson, A.D., 2013. Hydrogel-forming microneedle arrays exhibit antimicrobial properties: potential for enhanced patient safety. Int. J. Pharm. 451, 76–91.

Flaten, G.E., Palac, Z., Engesland, A., Filipović-Grčić, J., Vanić, Ž., Škalko-Basnet, N., 2015. In vitro skin models as a tool in optimization of drug formulation. Eur. J. Pharm. Sci. 75, 10–24.

Gallant, J.E., Thompson, M., DeJesus, E., Voskuhl, G.W., Wei, X., Zhang, H., White, K., Cheng, A., Quirk, E., Martin, H., 1988. Antiviral activity, safety, and pharmacokinetics of bictegravir as 10-day monotherapy in HIV-1–infected adults. J. Acquir. Immune Defic. Syndr. 75 (2017), 61–66.

Garland, M.J., Singh, T.R.R., Woolfson, A.D., Donnelly, R.F., 2011. Electrically enhanced solute permeation across poly(ethylene glycol)–crosslinked poly(methyl vinyl ether-co-maleic acid) hydrogels: effect of hydrogel crosslink density and ionic conductivity. Int. J. Pharm. 406, 91–98.

Global HIV and AIDS statistics. https://www.avert.org/global-hiv-and-aids-statistics (accessed January 6, 2022).

Gulsun, T., Borna, S.E., Vural, I., Sahin, S., 2018. Preparation and characterization of furosemide nanosuspensions. J. Drug Deliv. Sci. Technol. 45, 93–100.

Han, T., Das, D.B., 2015. Potential of combined ultrasound and microneedles for enhanced transdermal drug permeation: a review. Eur. J. Pharm. Biopharm. 89, 312–328.

Havlir, D., Gandhi, M., 2015. Implementation challenges for long-acting antivirals as treatment. Curr. Opin. HIV AIDS 10, 282–289.

He, J., Zhang, Z., Zheng, X., Li, L., Qi, J., Wu, W., Lu, Y., 2021. Design and evaluation of dissolving microneedles for enhanced dermal delivery of propranolol hydrochloride. Pharmaceutics. 13, 579–594.

Himawan, A., Anjani, Q.K., Detamornrat, U., Vora, L.K., Permana, A.D., Ghanma, R., Naser, Y., Rahmawanty, D., Scott, C.J., Donnelly, R.F., 2023. Multifunctional low temperature-cured PVA/PVP/citric acid-based hydrogel forming microarray patches: physicochemical characteristics and hydrophilic drug interaction. Eur. Polym. J. 186, 1–16.

K. Ahmed Saeed AL-Japairai, S. Mahmood, S. Hamed Almurisi, J. Reddy Venugopal, A. Rebhi Hilles, M. Azmana, S. Raman, Current trends in polymer microneedle for transdermal drug delivery, *Int J Pharm.* 587 (2020) 1–18.

Karakucuk, A., Celebi, N., 2020. Investigation of formulation and process parameters of wet media milling to develop etodolac nanosuspensions. Pharm. Res. 37, 1–18.

Khadka, P., Ro, J., Kim, H., Kim, I., Kim, J.T., Kim, H., Cho, J.M., Yun, G., Lee, J., 2014. Pharmaceutical particle technologies: an approach to improve drug solubility, dissolution and bioavailability. Asian J. Pharm. Sci. 9, 304–316.

Kharsany, A.B.M., Karim, Q.A., 2016. HIV infection and AIDS in sub-saharan africa: current status, challenges and opportunities. Open AIDS J. 10, 34–48.

Larrañeta, E., Moore, J., Vicente-Pérez, E.M., González-Vázquez, P., Lutton, R., Woolfson, A.D., Donnelly, R.F., 2014. A proposed model membrane and test method for microneedle insertion studies. Int. J. Pharm. 472, 65–73.

S.E. Lazerwith, R. Cai, X. Chen, G. Chin, M.C. Desai, S. Eng, R. Jacques, M. Ji, G. Jones, H. Martin, C. McMahon, M. Mish, P. Morganelli, J. Mwangi, H.-J. Pyun, U. Schmitz, G. Stepan, J. Szwarcberg, J. Tang, M. Tsiang, J. Wang, K. Wang, K. White, L. Wiser, J. Zack, H. Jin, Discovery of bictegravir (GS-9883), a novel, unboosted, once-daily HIV-1 integrase strand transfer inhibitor (INSTI) with improved pharmacokinetics and in vitro resistance profile. https://www.natap.org/2016/HIV/062016_05.htm (accessed May 15, 2022).

Li, W., Tang, J., Terry, R.N., Li, S., Brunie, A., Callahan, R.L., Noel, R.K., Rodríguez, C.A., Schwendeman, S.P., Prausnitz, M.R., 2019. Long-acting reversible contraception by effervescent microneedle patch. Sci. Adv. 5, 1–12.

Lu, C.H., Bednarczyk, E.M., Catanzaro, L.M., Shon, A., Xu, J.C., Ma, Q., 2021. Pharmacokinetic drug interactions of integrase strand transfer inhibitors. Curr. Res. Pharmacol. Drug Disc. 2, 1–8.

Malamatari, M., Taylor, K.M.G., Malamataris, S., Douroumis, D., Kachrimanis, K., 2018. Pharmaceutical nanocrystals: production by wet milling and applications. Drug Discov. Today 23, 534–547.

Mao, J., Wang, H., Xie, Y., Fu, Y., Li, Y., Liu, P., Du, H., Zhu, J., Dong, L., Hussain, M., Li, Y., Zhang, L., Zhu, J., Tao, J., 2020. Transdermal delivery of rapamycin with poor water-solubility by dissolving polymeric microneedles for anti-angiogenesis. J. Mater. Chem. B 8, 928–934.

Margolis, D.A., Gonzalez-Garcia, J., Stellbrink, H.J., Eron, J.J., Yazdanpanah, Y., Podzamczer, D., Lutz, T., Angel, J.B., Richmond, G.J., Clotet, B., Gutierrez, F., Sloan, L., Clair, M.S., Murray, M., Ford, S.L., Mrus, J., Patel, P., Crauwels, H., Griffith, S.K., Sutton, K.C., Dorey, D., Smith, K.Y., Williams, P.E., Spreen, W.R., 2017. Long-acting intramuscular cabotegravir and rilpivirine in adults with HIV-1 infection (LATTE-2): 96-week results of a randomised, open-label, phase 2b, non-inferiority trial. Lancet 390, 1499–1510.

Mayer, K.H., Venkatesh, K.K., 2010. Antiretroviral therapy as HIV prevention: status and prospects. Am. J. Public Health 100, 1867–1876.
Mc Crudden, M.T.C., Larrañeta, E., Clark, A., Jarrahian, C., Rein-Weston, A., Lachau-Durand, S., Niemeijer, N., Williams, P., Haeck, C., McCarthy, H.O., Zehrung, D., Donnelly, R.F., 2018. Design, formulation and evaluation of novel dissolving microarray patches containing a long-acting rilpivirine nanosuspension. J. Control. Release 292, 119–129.
McAlister, E., Kirkby, M., Domínguez-Robles, J., Paredes, A.J., Anjani, Q.K., Moffatt, K., Vora, L.K., Hutton, A.R.J., McKenna, P.E., Larrañeta, E., Donnelly, R.F., 2021. The role of microneedle arrays in drug delivery and patient monitoring to prevent diabetes induced fibrosis. Adv. Drug Deliv. Rev. 175, 1–29.
McGuckin, M.B., Wang, J., Ghanma, R., Qin, N., Palma, S.D., Donnelly, R.F., Paredes, A. J., 2022. Nanocrystals as a master key to deliver hydrophobic drugs via multiple administration routes. J. Control. Release 345, 334–353.
Moffatt, K., Tekko, I.A., Vora, L., Volpe-Zanutto, F., Hutton, A.R.J., Mistilis, J., Jarrahian, C., Akhavein, N., Weber, A.D., McCarthy, H.O., Donnelly, R.F., 2022. Development and evaluation of dissolving microarray patches for co-administered and repeated intradermal delivery of long-acting rilpivirine and cabotegravir nanosuspensions for pediatric HIV antiretroviral therapy. Pharm. Res. 1, 1–24.
Naser, Y.A., Tekko, I.A., Vora, L.K., Peng, K., Anjani, Q.K., Greer, B., Elliott, C., McCarthy, H.O., Donnelly, R.F., 2023. Hydrogel-forming microarray patches with solid dispersion reservoirs for transdermal long-acting microdepot delivery of a hydrophobic drug. J. Control. Release 356, 416–433.
Nasiri, M.I., Vora, L.K., Ershaid, J.A., Peng, K., Tekko, I.A., Donnelly, R.F., 2022. Nanoemulsion-based dissolving microneedle arrays for enhanced intradermal and transdermal delivery. Drug Deliv Transl. Res. 12, 881–896.
Nguyen, H.X., Bozorg, B.D., Kim, Y., Wieber, A., Birk, G., Lubda, D., Banga, A.K., 2018. Poly (vinyl alcohol) microneedles: fabrication, characterization, and application for transdermal drug delivery of doxorubicin. Eur. J. Pharm. Biopharm. 129, 88–103.
Palk, L., Okano, J.T., Dullie, L., Blower, S., 2020. Travel time to health-care facilities, mode of transportation, and HIV elimination in Malawi: a geospatial modelling analysis. Lancet Glob Health 8, 1555–1564.
Paredes, A.J., Volpe-Zanutto, F., Permana, A.D., Murphy, A.J., Picco, C.J., Vora, L.K., Coulter, J.A., Donnelly, R.F., 2021. Novel tip-loaded dissolving and implantable microneedle array patches for sustained release of finasteride. Int. J. Pharm. 606, 1–12.
Paredes, A.J., Permana, A.D., Volpe-Zanutto, F., Amir, M.N., Vora, L.K., Tekko, I.A., Akhavein, N., Weber, A.D., Larrañeta, E., Donnelly, R.F., 2022. Ring inserts as a useful strategy to prepare tip-loaded microneedles for long-acting drug delivery with application in HIV pre-exposure prophylaxis. Mater. Des. 224, 1–11.
Permana, A.D., McCrudden, M.T.C., Donnelly, R.F., 2019. Enhanced intradermal delivery of nanosuspensions of antifilariasis drugs using dissolving microneedles: a proof of concept study. Pharmaceutics. 11, 1–22.
Permana, A.D., Paredes, A.J., Volpe-Zanutto, F., Kurnia Anjani, Q., Utomo, E., Donnelly, R.F., 2020. Dissolving microneedle-mediated dermal delivery of itraconazole nanocrystals for improved treatment of cutaneous candidiasis. Eur. J. Pharm. Biopharm. 154, 50–61.
Plakkot, S., de Matas, M., York, P., Saunders, M., Sulaiman, B., 2011. Comminution of ibuprofen to produce nanoparticles for rapid dissolution. Int. J. Pharm. 415, 307–314.
Rabiei, M., Kashanian, S., Bahrami, G., Derakhshankhah, H., Barzegari, E., Samavati, S. S., McInnes, S.J.P., 2021. Dissolving microneedle-assisted long-acting Liraglutide delivery to control type 2 diabetes and obesity. Eur. J. Pharm. Sci. 167, 1–9.
Ramöller, I.K., Abbate, M.T.A., Vora, L.K., Hutton, A.R.J., Peng, K., Volpe-Zanutto, F., Tekko, I.A., Moffatt, K., Paredes, A.J., McCarthy, H.O., Donnelly, R.F., 2022. HPLC-MS method for simultaneous quantification of the antiretroviral agents rilpivirine and cabotegravir in rat plasma and tissues. J. Pharm. Biomed. Anal. 213, 1–10.
Ripolin, A., Quinn, J., Larrañeta, E., Vicente-Perez, E.M., Barry, J., Donnelly, R.F., 2017. Successful application of large microneedle patches by human volunteers. Int. J. Pharm. 521, 92–101.
Rojekar, S., Vora, L.K., Tekko, I.A., Volpe-Zanutto, F., McCarthy, H.O., Vavia, P.R., Ryan, R.F., 2021. Etravirine-loaded dissolving microneedle arrays for long-acting delivery. Eur. J. Pharm. Biopharm. 165, 41–51.
Saxena, P., Shukla, P., Gaur, M.S., 2020. Thermal analysis of polymer blends and double layer by DSC. Polym. Polym. Compos. 29, 11–18.
Summerfield, A., Meurens, F., Ricklin, M.E., 2015. The immunology of the porcine skin and its value as a model for human skin. Mol. Immunol. 66, 14–21.
Surve, D.H., Jindal, A.B., 2020. Recent advances in long-acting nanoformulations for delivery of antiretroviral drugs. J. Control. Release 324, 379–404.
Swindells, S., Andrade-Villanueva, J.-F., Richmond, G.J., Rizzardini, G., Baumgarten, A., Masiá, M., Latiff, G., Pokrovsky, V., Bredeek, F., Smith, G., Cahn, P., Kim, Y.-S., Ford, S.L., Talarico, C.L., Patel, P., Chounta, V., Crauwels, H., Parys, W., Vanveggel, S., Mrus, J., Huang, J., Harrington, C.M., Hudson, K.J., Margolis, D.A., Smith, K.Y., Williams, P.E., Spreen, W.R., 2020. Long-acting cabotegravir and rilpivirine for maintenance of HIV-1 suppression. N. Engl. J. Med. 382, 1112–1123.
Tekko, I.A., Permana, A.D., Vora, L., Hatahet, T., McCarthy, H.O., Donnelly, R.F., 2020. Localised and sustained intradermal delivery of methotrexate using nanocrystal-loaded microneedle arrays: potential for enhanced treatment of psoriasis. Eur. J. Pharm. Sci. 152, 1–16.
Tekko, I.A., Vora, L.K., Volpe-Zanutto, F., Moffatt, K., Jarrahian, C., McCarthy, H.O., Donnelly, R.F., Tekko, I.A., Vora, L.K., Volpe-Zanutto, F., Moffatt, K., McCarthy, H. O., Donnelly, R.F., 2022. Novel bilayer microarray patch-assisted long-acting micro-depot cabotegravir intradermal delivery for HIV pre-exposure prophylaxis. Adv. Funct. Mater. 32, 2270059–2270077.
Thoueille, P., Choong, E., Cavassini, M., Buclin, T., Decosterd, L.A., 2022. Long-acting antiretrovirals: a new era for the management and prevention of HIV infection. J. Antimicrob. Chemother. 77, 290–302.
Vlahov, D., Robertson, A.M., Strathdee, S.A., 2010. Prevention of HIV infection among injection drug users in resource-limited settings. Clin. Infect. Dis. 50, 114–121.
Volpe-Zanutto, F., Vora, L.K., Tekko, I.A., McKenna, P.E., Permana, A.D., Sabri, A.H., Anjani, Q.K., McCarthy, H.O., Paredes, A.J., Donnelly, R.F., 2022. Hydrogel-forming microarray patches with cyclodextrin drug reservoirs for long-acting delivery of poorly soluble cabotegravir sodium for HIV pre-exposure prophylaxis. J. Control. Release 348, 771–785.
L.K. Vora, K. Moffatt, I.A. Tekko, A.J. Paredes, F. Volpe-Zanutto, D. Mishra, K. Peng, R. Raj Singh Thakur, R.F. Donnelly, Microneedle array systems for long-acting drug delivery, *European Journal of Pharmaceutics and Biopharmaceutics*. 159 (2021) 44–76.
Vora, L.K., Vavia, P.R., Larrañeta, E., Bell, S.E.J., Donnelly, R.F., 2018. Novel nanosuspension-based dissolving microneedle arrays for transdermal delivery of a hydrophobic drug. J. Interdiscip. Nanomed. 3, 89–101.
Vora, L.K., Moffatt, K., Donnelly, R.F., 2022. Long-lasting drug delivery systems based on microneedles. Long-acting Drug Delivery Systems: Pharmaceutical, Clinical, and Regulatory Aspects 9, 249–287.
Wong, J.K., Yukl, S.A., 2016. Tissue reservoirs of HIV. Curr. Opin. HIV AIDS 11, 262–370.